



PAPER

Higher-eigenmode piezoresponse force microscopy: a path towards increased sensitivity and the elimination of electrostatic artifacts

RECEIVED
29 December 2017REVISED
6 February 2018ACCEPTED FOR PUBLICATION
28 February 2018PUBLISHED
23 March 2018

Gordon A MacDonald, Frank W DelRio and Jason P Killgore

Material Measurement Laboratory, National Institute of Standards and Technology, Boulder, CO, United States of America

E-mail: jason.killgore@nist.gov**Keywords:** piezoresponse force microscopy, atomic force microscopy, ferroelectricSupplementary material for this article is available [online](#)**Abstract**

Piezoresponse force microscopy (PFM) and related bias-induced strain sensing atomic force microscopy techniques provide unique characterization of material-functionality at the nanoscale. However, these techniques are prone to unwanted artifact signals that influence the vibration amplitude of the detecting cantilever. Here, we show that higher-order contact resonance eigenmodes can be readily excited in PFM. The benefits of using the higher-order eigenmodes include absolute sensitivity enhancement, electrostatic artifact reduction, and lateral versus normal strain decoupling. This approach can significantly increase the proportion of total signal arising from desired strain (as opposed to non-strain artifacts) in measurements with cantilevers exhibiting typical, few N m^{-1} spring constants to cantilevers up to $1000\times$ softer than typically used.

Introduction

In piezoresponse force microscopy (PFM), and related techniques, an AC voltage (V_{AC}) is applied between an atomic force microscopy (AFM) probe and the sample of interest. The electro-mechanical deformation of the surface, as well as various unwanted processes, cause vibration of the AFM probe which is detected by the AFM system. To date, measurements have been taken almost exclusively at or below the first flexural contact resonance frequency, f_1^c . These techniques are of wide interest to material scientists due to the unparalleled lateral resolution they afford for studying the electromechanical properties of several classes of applied material systems [1]. Applied materials that exhibit an electromechanical response include piezoelectric materials relevant to transducers, actuators, and piezoelectric energy harvesting structures, ferroelectric materials relevant to non-volatile memory storage, emerging organic–inorganic perovskite photovoltaic active layers, and even some biological materials [1–3]. With the recent Nobel prize award in molecular electromechanical machines [4], PFM is expected to play a critical role in studying the response of these systems at the device and assembly level [1]. The closely related method of electrochemical-strain microscopy has been used to study solid-state battery materials [5, 6]. Despite the widespread interest in and adoption of PFM and related techniques by the scientific community over the past two decades, these measurements are susceptible to a number of measurement artifacts [1], leading to results that appear paradoxical, e.g. the apparent piezoelectric response and/or ferroelectric writing of materials that are known to be neither piezoelectric nor ferroelectric [7, 8]. These artifacts are widely attributed to tip electrostatic (TES) forces between the tip and sample (F_{TES}), and body electrostatic (BES) forces that operate non-locally between the cantilever body and sample (F_{BES}) as shown in figure 1. Some of the artifacts can be reduced by operating with stiff cantilevers or tall tips [9]. Such approaches lead to compromises in the ability to investigate fragile specimens without damage, and limit the diversity of cantilever types that can be used. As such, more universal methods of artifact minimization and PFM signal maximization are desired.

Based on recent experimental results in contact resonance force microscopy, a nanomechanical measurement method, the use of higher eigenmodes (i.e. resonant vibrational modes) of a cantilever can result in an improved sensitivity of resonance frequency to contact stiffness, reduced influence of poorly-known lateral

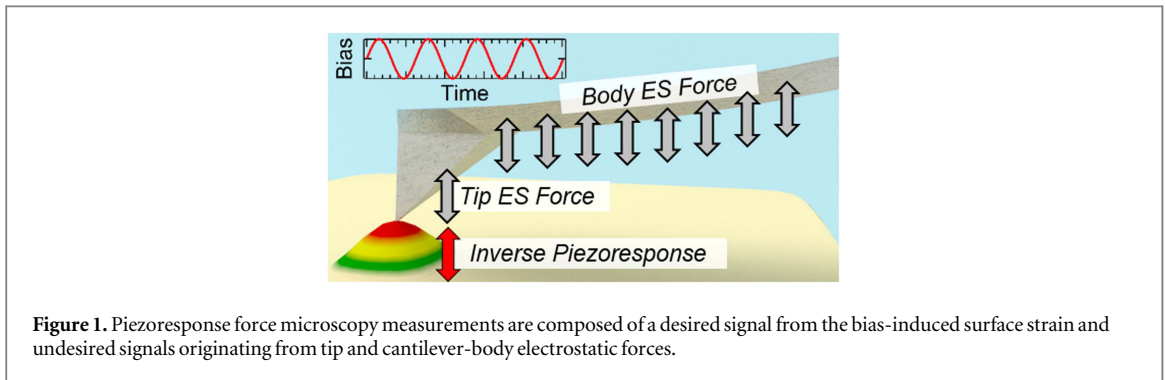


Figure 1. Piezoresponse force microscopy measurements are composed of a desired signal from the bias-induced surface strain and undesired signals originating from tip and cantilever-body electrostatic forces.

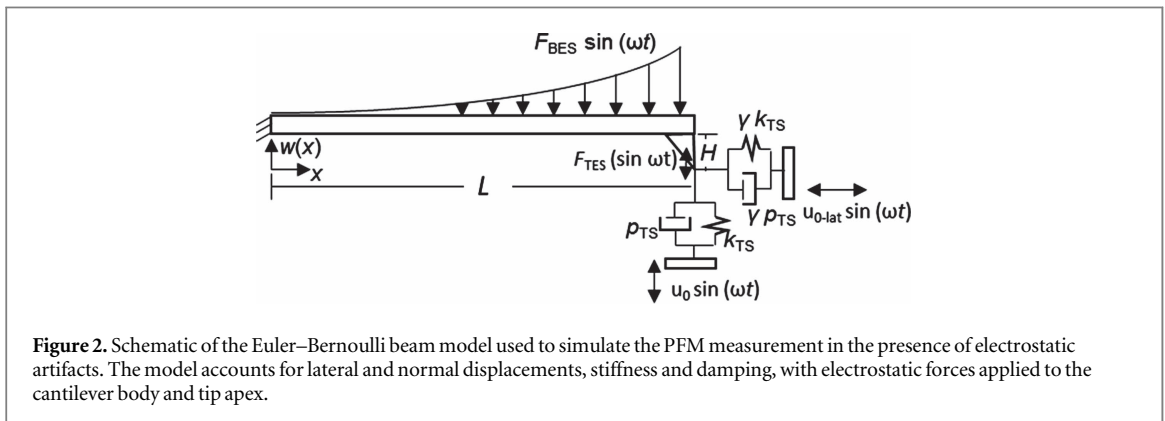


Figure 2. Schematic of the Euler–Bernoulli beam model used to simulate the PFM measurement in the presence of electrostatic artifacts. The model accounts for lateral and normal displacements, stiffness and damping, with electrostatic forces applied to the cantilever body and tip apex.

deformations, and the ability to operate with cantilevers of reduced quasistatic spring constant (k_{cant}) compared to the cantilever types that have been traditionally used on similar classes of materials [10]. In that work, many of the benefits were ascribed to the higher dynamic stiffness [11] associated with the higher eigenmodes. Higher eigenmodes should be accessible in PFM, and the increased dynamic stiffness of the higher modes is a promising mechanism to reduce the influence of F_{BES} . The potential for reducing electrostatic artifacts by using higher frequencies for PFM measurements, both off resonance and on resonance, has been suggested in previous work [12, 13]. In this study, we demonstrate that usage of the higher CR modes of a cantilever not only dramatically reduces the influence of non-local electrostatic forces, but also enhances the sensitivity to small PFM signals and allows for tailoring of the sensitivity to non-normal displacements arising from cantilever tilt or tilted piezoelectric domains. Experimental results comparing higher eigenmode CR frequencies (f_n^c , $n > 1$) to results obtained at f_1^c on periodically-poled lithium niobate (PPLN) exhibit improved agreement with the expected 180° phase shift between Up and Down domains as n is increased. We also show that varying the DC bias between the tip and sample ($k_{cant} \approx 0.3 \text{ N m}^{-1}$) results in varying magnitudes of electrostatic artifact for the first eigenmode, but the effect of varying the DC bias is negligible for higher-order eigenmodes. The ratio of the observed amplitude associated with the desired surface strain is compared to the amplitude associated with the artifacts, and whereas as little as 10% of the observed amplitude may arise from surface strain in the first eigenmode, more than 90% of the observed signal is driven by surface strain at the fifth eigenmode. The higher eigenmode approach is further extended to a cantilever $1000\times$ softer than the status quo in typical PFM, while still yielding reliable phase results and amplitude contrast comparable to the results obtained with f_1^c for the status quo probe. Overall, our approach allows for cantilever selection to be optimized for image quality and spatial resolution, without compromising the reliability of the PFM measurement.

Methods

Theoretical modeling of PFM with measurement artifacts for various contact resonant modes

To understand how PFM measurements are affected at higher flexural eigenmodes, the cantilever-sample system was modeled using the well-established Euler–Bernoulli beam theory. A schematic of the particular model, which is simplified slightly from that presented recently by Bradler-Rohling *et al* [14] is shown in figure 2. The model includes the effects of normal tip-sample stiffness k_{TS} and damping p_{TS} , ratio of normal to lateral stiffness and damping γ , surface normal displacement u_0 , surface lateral displacement u_{0-lat} , a non-local electrostatic force acting on the cantilever body $F_{BES}(x)$, and a localized electrostatic force acting at the cantilever

tip F_{TES} . Note that the surface displacement and electrostatic force parameters u_0 , $u_{0\text{-lat}}$, $F_{\text{BES}}(x)$, and F_{TES} are periodic piezoelectric and electrostatic responses to the applied AC voltage at frequency ω .

After separating out the time-dependent response, the amplitude of the cantilever $w(x)$ is described by

$$\frac{\partial^4 w}{\partial x^4} - \frac{F_{\text{BES}}(x)}{EI} = \beta^4 w(x), \quad (1)$$

where x is the position along the cantilever, E is the Young's modulus, and I is the bending moment of inertia. The value of β is a function of frequency f given by

$$\beta = \frac{x_1^0}{L} \left(\left(\frac{f}{f_1^0} \right)^2 + i \left(\frac{1}{Q_{\text{free}}} \frac{f}{f_1^0} \right) \right)^{1/4}, \quad (2)$$

where $x_1^0 = 1.8751$, L is the cantilever length, f_1^0 is the first free resonance frequency, and Q_{free} is the quality factor of the first free resonance.

$F_{\text{BES}}(x)$ decays away from the tip due to the increasing cantilever-sample distance $d(x)$ resulting from the cantilever tilt relative to the sample surface. The distance $d(x)$ is given by

$$d(x) = H \cos(\zeta) + (L - x) \sin(\zeta), \quad (3)$$

where H is the height of the AFM tip, L is the cantilever length, and ζ is the tilt angle. Based on a tilted parallel plate capacitor, $F_{\text{BES}}(x)$ is given by

$$F_{\text{BES}}(x) = \frac{-\cos(\zeta) \varepsilon_0 \varepsilon_r V_{\text{AC}} b \Delta V}{d(x)^2} = \frac{q_0 \Delta V}{d(x)^2}, \quad (4)$$

where ε_0 is the permittivity of free space, ε_r is the relative permittivity, $V_{\text{AC}} = 3$ V is the applied AC voltage, b is the cantilever width, and ΔV is the contact potential difference between the probe body and sample surface. For practical purposes, the constants in the numerator of equation (4) were lumped together and into q_0 . ΔV was then adjusted to match experimental and theoretical amplitudes of the first free resonance when the AFM tip was 200 nm from the sample surface ($\Delta V = 5.45$ V, $q_0 = -7.82 \times 10^{-16}$ N m² V⁻¹).

The boundary conditions for equation (1) were set as shown in figure 2. i.e.

no displacement at the cantilever base,

$$w(0) = 0, \quad (5)$$

no slope at the cantilever base,

$$w'(0) = 0, \quad (6)$$

a bending moment at the tip from the lateral contact force, coupled through the tip-height,

$$w''(L) = \frac{\psi}{L^3} \gamma H (u_{0\text{-lat}} - w'(L)H), \quad (7)$$

a shear force at the tip from the normal contact force and the local TES force,

$$w'''(L) = \frac{\psi}{L^3} (w(L) - u_0) - 3F_{\text{TES}} / (k_{\text{cant}} L^3), \quad (8)$$

where ψ is the contact function $\psi = 3k_{\text{TS}}/k_{\text{cant}} + i(\beta L)^2 p_{\text{TS}}$.

Finally, the AFM operates as a slope sensitive amplitude detector, thus the relevant amplitude signal A_{AFM} is given by $A_{\text{AFM}}(x) = |w'(x)|$, although the experimental signal will also have some spatial averaging due to the finite size of the detection laser spot. The parameters used in the simulations are given in table 1.

Imaging and point spectral acquisition of PFM data for lower- and higher-order eigenmodes

PFM was performed on a Cypher AFM (Asylum Research, Santa Barbara, CA). Measurements were performed in air with a variety of metal-coated probes with a wide range of k_{cant} . These included a 'status quo' probe typical of the probes used for PFM measurements (Asyelec-01, Asylum Research, $k_{\text{cant}} \approx 2$ N m⁻¹), a 'soft' probe (ContPT, NanoWorld, $k_{\text{cant}} \approx 0.2$ N m⁻¹), and an 'ultra-soft' probe (Biolever, Olympus, $k_{\text{cant}} \approx 0.006$ N m⁻¹). The laser spot position on the cantilever was precisely calibrated for all measurements (see supplementary information available online at stacks.iop.org/NANOF/2/015005/mmedia: Laser Position Calibration). AC and DC bias voltage were applied to the cantilever spring clip, while the sample shared a common ground. AC and DC bias voltages were kept at values far below the polarization voltage of Lithium Niobate [15] and drive frequencies were considerably below the reported response frequencies of the material [16]. All images were acquired in dual AC resonance tracking (DART) PFM mode. Point amplitude versus frequency spectra were fit to a simple harmonic oscillator (SHO) model using a custom script in Igor Pro (Wavemetrics, Portland, OR) scientific graphing and data analysis software.

Table 1. Parameter values used in the PFM simulations with and without artifacts.

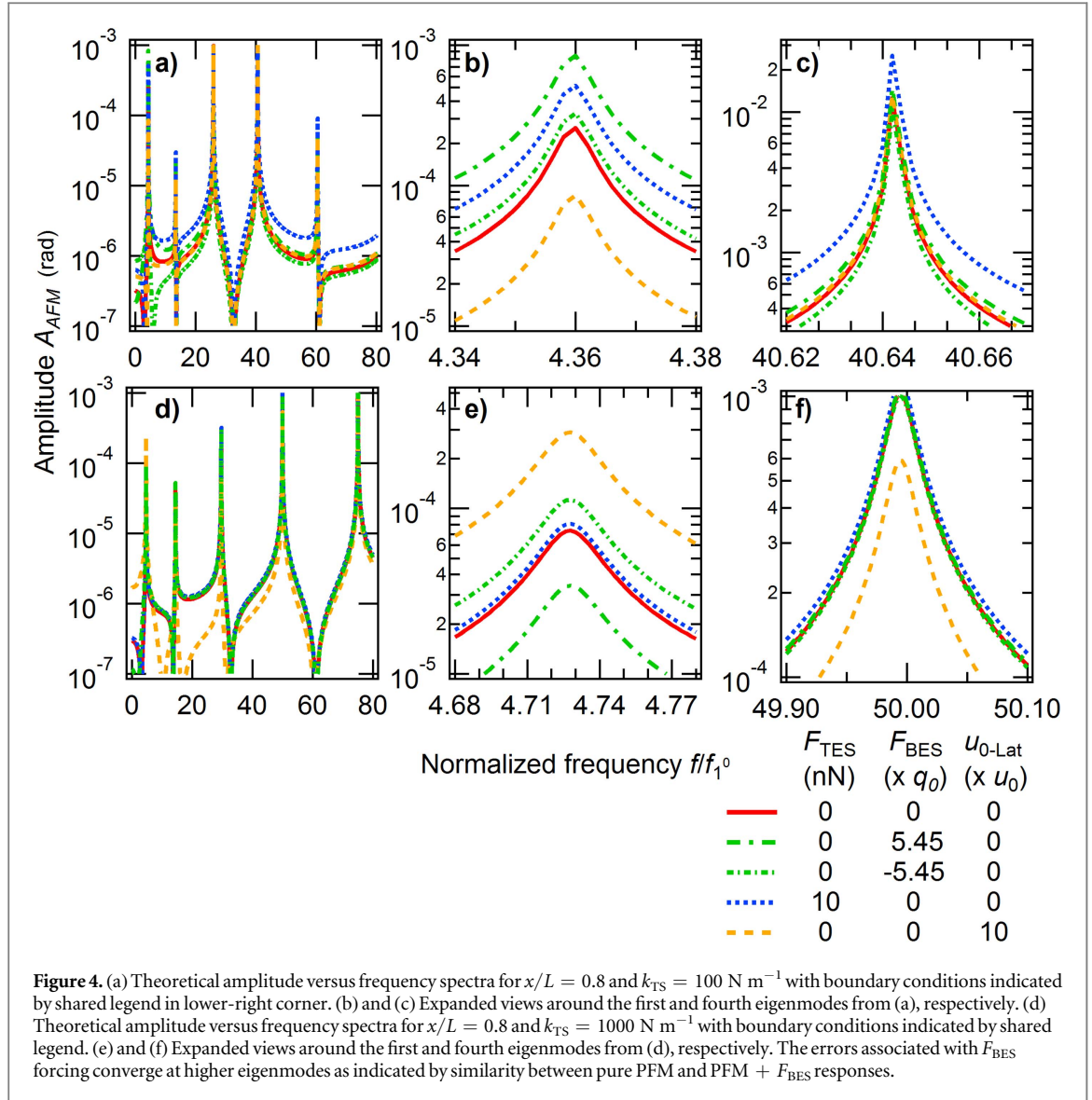
Quantity	Values
k_{cant}	{0.3, 3} N m ⁻¹
Q_{free}	43.5
L	450 μm
H	6 μm
ζ	11°
k_{TS}	{100, 1000} N m ⁻¹
p_{ts}	0
γ	0.8
u_0	10 pm
$u_{0\text{-lat}}$	{0, 10} pm
ΔV	{0, 5.45} V
q_0	-7.82×10^{-16} N m ² V ⁻¹
F_{TES}	{0, 10} nN

Results and discussion

Prediction of enhanced sensitivity and reduced measurement artifacts with higher-eigenmode PFM

For nanomechanical property sensing, operation at higher eigenmodes has been shown to increase the sensitivity of the CR frequency to sample stiffness changes [10]. Here, we address the question of how the detection sensitivity of a pure normal PFM signal (i.e., $F_{\text{TES}} = 0$, $F_{\text{BES}}(x) = 0$, $u_{0\text{-lat}} = 0$) varies with eigenmode order n . In figure 3, we demonstrate the impact of eigenmode order on PFM amplitude with a PFM strain set to $u_0 = 100$ pm. Plots of A_{AFM} versus the relative detection spot position (x/L) for the first 5 eigenmodes of a 0.3 N m⁻¹ cantilever at (a) $k_{\text{TS}} = 100$ N m⁻¹ and (b) $k_{\text{TS}} = 1000$ N m⁻¹ are shown. In both cases, the largest maximum amplitude signal does *not* occur at f_1^c . At $k_{\text{TS}} = 100$ N m⁻¹, modes 4 and 5 show similar maximum sensitivities (maximum amplitude of modes 4 and 5 is 8.4×10^{-4} rad) which is an order of magnitude greater than the maximum amplitude signal of mode 1 (8.2×10^{-5} rad). At $k_{\text{TS}} = 1000$ N m⁻¹, mode 5 is most sensitive (maximum amplitude of 1.8×10^{-3} rad). In an experiment, the signal amplitude will depend on the laser spot position on the cantilever due to shape factor effects (i.e., the laser spot position may coincide with any value of x/L shown in figure 3), but this result indicates that the maximum signal amplitude, with optimized laser position, is higher for the higher order modes. It is well known that the interaction of the cantilever with the surrounding environment leads to an increased damping of the cantilever vibration with increasing frequency; this frequency-dependent damping is included in the modeling results in figures 3(a) and (b). The increased sensitivity with increasing eigenmode order arises, in part, from additional tip-sample indentation due to the increased dynamic stiffness of the higher eigenmodes. This increased indentation is a sufficiently large effect to overcome the loss in amplitude that arises from environmental damping effects. Thus, for the purposes of amplifying small surface-strain signals on materials that are stiff relative to the static cantilever spring constant, higher modes are an attractive option. Figure 3(c) shows analogous results to figure 3(a), but with a constant damping ratio which could occur for experimental conditions where frequency-independent material damping dominates the response rather than frequency-dependent environmental or material damping (e.g., measurements on rigid inorganic materials in vacuum). The increase in maximum PFM amplitude with mode order is seen to be larger for frequency-independent damping (figure 3(c)) than for frequency-dependent damping (figures 3(a) and (b)). This ability for higher modes to amplify the piezoresponse signal will benefit PFM applications where the magnitude of the piezoresponse is small, such as ultra-thin films or materials with small piezoelectric coefficients.

In addition to the desired PFM response induced by a strain normal to the sample surface, we also simulated the influence of parasitic electrostatic forces arising between the sample and cantilever body (F_{BES}) and tip (F_{TES}) and buckling displacements ($u_{0\text{-lat}}$) that originate from tilted sample domains and/or cantilever-sample tilt. Figures 4(a) and (d) show simulated amplitude versus frequency spectra acquired with the laser position at $x/L = 0.8$ and normal tip sample stiffness of either $k_{\text{TS}} = 100$ N m⁻¹ or $k_{\text{TS}} = 1000$ N m⁻¹ under various boundary conditions. This value of x/L was chosen because it coincides with the fourth (closest to tip) antinode of the fifth free resonance and there is a simple procedure for setting the laser position to precisely match an antinode of a free resonance (see supplementary information: Laser Position Calibration). The value for k_{TS} is of the order calculated from the experimental contact resonance frequencies, and is typical of contact AFM measurements with soft or moderately stiff cantilevers on rigid inorganic substrates. The conditions simulated include: (1) a pure, normal piezoresponse, (2) a normal piezoresponse plus the influence of a BES force (either

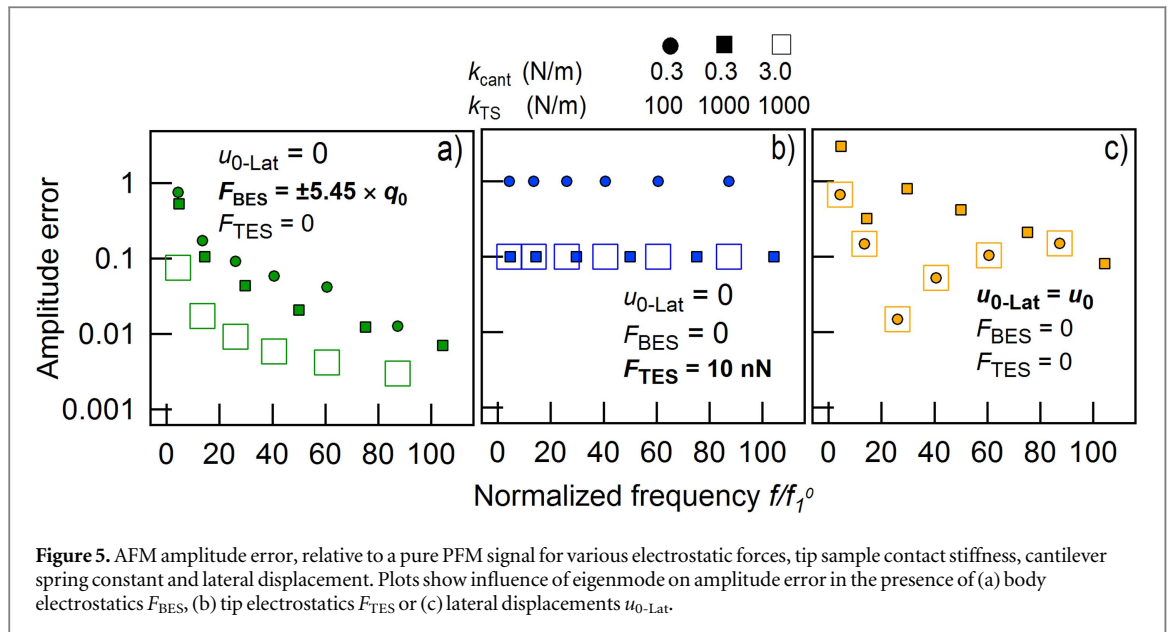


quantification of the surface strain from PFM amplitude measurements is a more tractable problem for on-resonance conditions than off-resonance.

Figure 5 shows the error between the total, on resonance, AFM amplitude A_{total} including additional drive forces, and a signal due to a pure normal piezoresponse A_{piezo} . Where,

$$\text{Amplitude error} = \left| \frac{A_{total} - A_{piezo}}{A_{piezo}} \right|. \quad (9)$$

The amplitude error introduced by the non-local BES force in figure 5(a) is seen to decrease exponentially with increasing eigenmode. With increasing eigenmode, the number of nodes in the vibrational shape also increase. Thus, there are more points along the cantilever body where the BES force results in zero displacement. Resultantly, each of the cantilever segments between the nodes exhibits a reduced span, giving it a higher dynamic stiffness. For a given eigenmode, the effects of BES forces are further mitigated by increasing contact stiffness because the tip-sample contact becomes more node-like as well. For the simulated conditions, the reduction in error with increased k_{TS} is greatest for the 5th eigenmode, where amplitude error decreases by 70% when increasing k_{TS} 10-fold at constant k_{cant} . This coincides with the 5th eigenmode exhibiting the largest percent-increase in frequency for the 10-fold stiffness increase. Increasing the quasistatic spring constant of the cantilever is also effective at reducing the BES artifact, though experimentally this comes at the expense of force control. Notably, using the 3rd or higher eigenmode of the $k_{cant} = 0.3 \text{ N m}^{-1}$ lever results in lower amplitude error than the 1st eigenmode of the $k_{cant} = 3.0 \text{ N m}^{-1}$ cantilever, and the additional benefit of a $10 \times$ increase in force control. In contrast to the non-local force, the influence of local tip-electrostatic force, figure 5(b), is linearly dependent on normalized tip-sample contact stiffness k_{TS}/k_{cant} and independent of eigenmode. Finally,



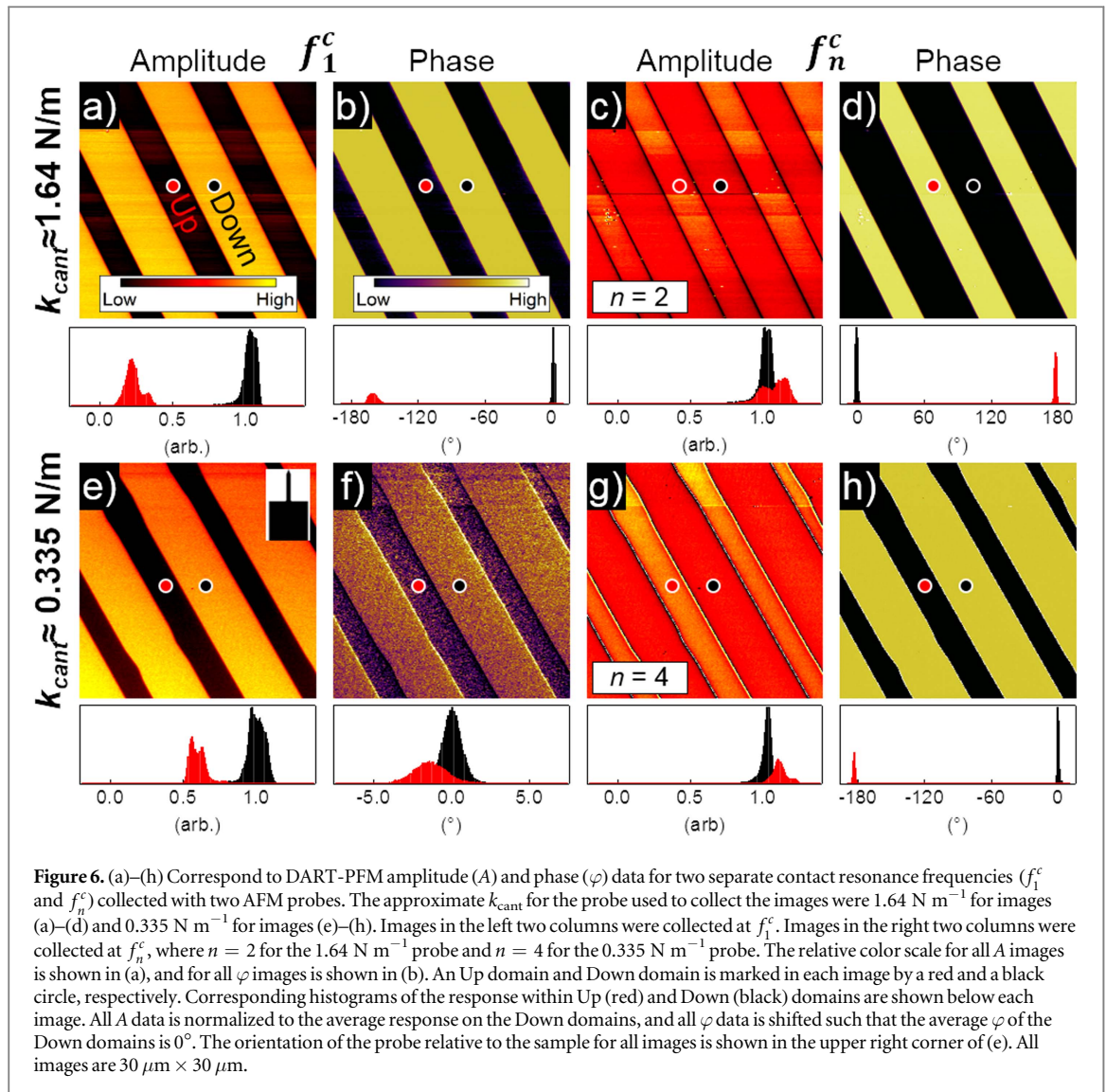
the sensitivity to lateral buckling displacements in figure 5(c) shows a nonmonotonic variation with increasing eigenmode order. This corresponds with coupling of the lateral surface strain u_0 with the tip-motion prescribed by the eigenmode. A benefit of the observed dependence is the ability to operate at eigenmodes that either *enhance or suppress* the influence of the lateral motion, while still having sufficient dynamic stiffness to suppress BES forces. Thus, using higher modes for PFM measurements can be a means to separate the contributions of the normal and lateral piezoresponse without the qualitative approach of changing the probe-sample orientation, or deconvolving the vertical and lateral AFM signals [18].

For all parameters, the comparison between $k_{TS} = 100 \text{ N m}^{-1}$ and $k_{TS} = 1000 \text{ N m}^{-1}$ provides an interesting basis for comparison. The value of k_{TS} can be readily adjusted by varying the quasistatic setpoint force or intentionally increasing the radius of the tip through wear. The higher value of k_{TS} will lead to reduced body and TES contribution at all eigenmodes, but could either enhance or suppress the sensitivity to $u_{0\text{-Lat}}$. Having demonstrated the benefits of higher eigenmodes for PFM measurements from a theoretical standpoint, we now demonstrate these benefits experimentally.

Evaluating the influence of higher eigenmodes on experimental PFM data with varied cantilever spring constants and electrostatic artifacts

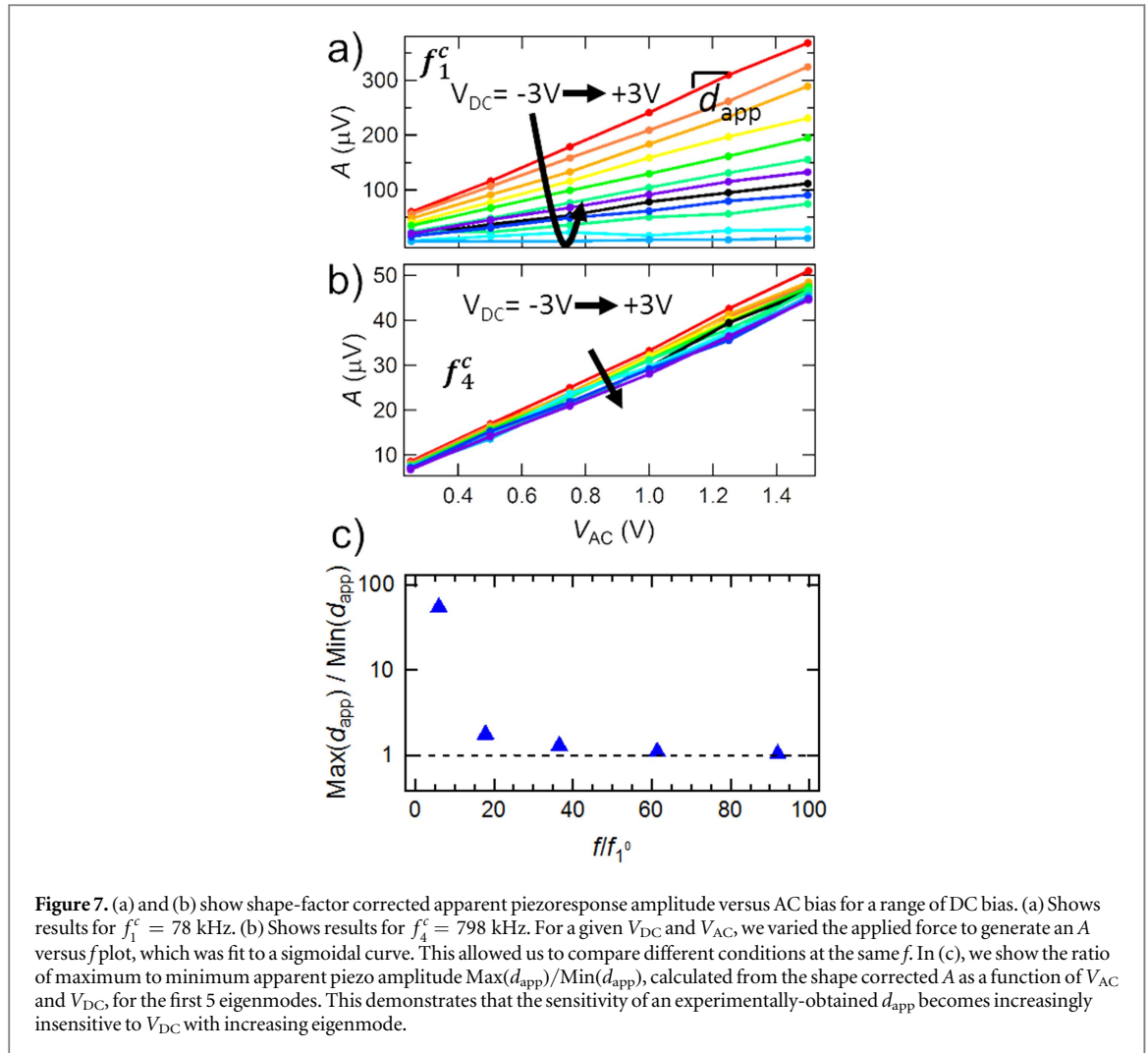
To demonstrate the effects of using higher-order contact-resonance frequencies for PFM measurements, we collected data on a PPLN sample with a variety of cantilevers using DART-PFM imaging [19]. Data was post-processed by fitting amplitude, phase, and frequency response to a SHO model to determine resonance frequency, quality factor, drive amplitude, and drive phase [20]. The ideal PFM response for this PPLN sample (i.e., in the absence of confounding effects such as electrostatic forces or lateral strains) is amplitude contrast $\Delta A = 0$ and phase shift $\Delta\varphi = 180^\circ$ between Up and Down domains [21]. This is under the assumption that the only physical property that changes with periodic poling is the orientation of the piezoelectric dipole (either $+c$ or $-c$ direction). The PFM data shown in figures 6(a) and (b), which were collected at f_1^c ($\sim 267 \text{ kHz}$) for the $k_{\text{cant}} = 1.64 \text{ nN nm}^{-1}$ probe, represents PFM results on a highly ideal sample using a probe with k_{cant} in a range ‘typical’ for PFM measurements in the literature [9, 14, 21, 22]. We observe considerable artifacts in the result, even for this status-quo measurement. This is most evident in the amplitude A response, where there is a $77\% \pm 7\%$ larger amplitude on the Down domains compared to the Up domains. The $\Delta\varphi$ between the Up and Down domains ($162^\circ \pm 5^\circ$), which shows a strong contrast, still falls short of the expected $\Delta\varphi = 180^\circ$.

In figures 6(c) and (d), the DART-PFM responses at f_2^c ($\approx 837 \text{ kHz}$) are shown. Results collected at this higher resonant mode are much closer to the ideal results. The A responses of the Up and Down domains are equivalent within statistical uncertainty ($\Delta A = 7\% \pm 15\%$, with the average A value slightly smaller on the Down domains), and the observed $\Delta\varphi$ is $179^\circ \pm 2^\circ$, in excellent agreement with the ideal response. Thus, we have demonstrated that the measured PFM response is significantly different from the ideal response (due to artifacts such as electrostatic forces and lateral surface strain) when using a probe and resonant mode that is ‘typical’ of the measurements in the literature to-date. Furthermore, we have demonstrated that performing the measurement at the second rather than first contact resonance mode, without any other changes to the experimental procedure or hardware, minimizes the influence of measurement artifacts.



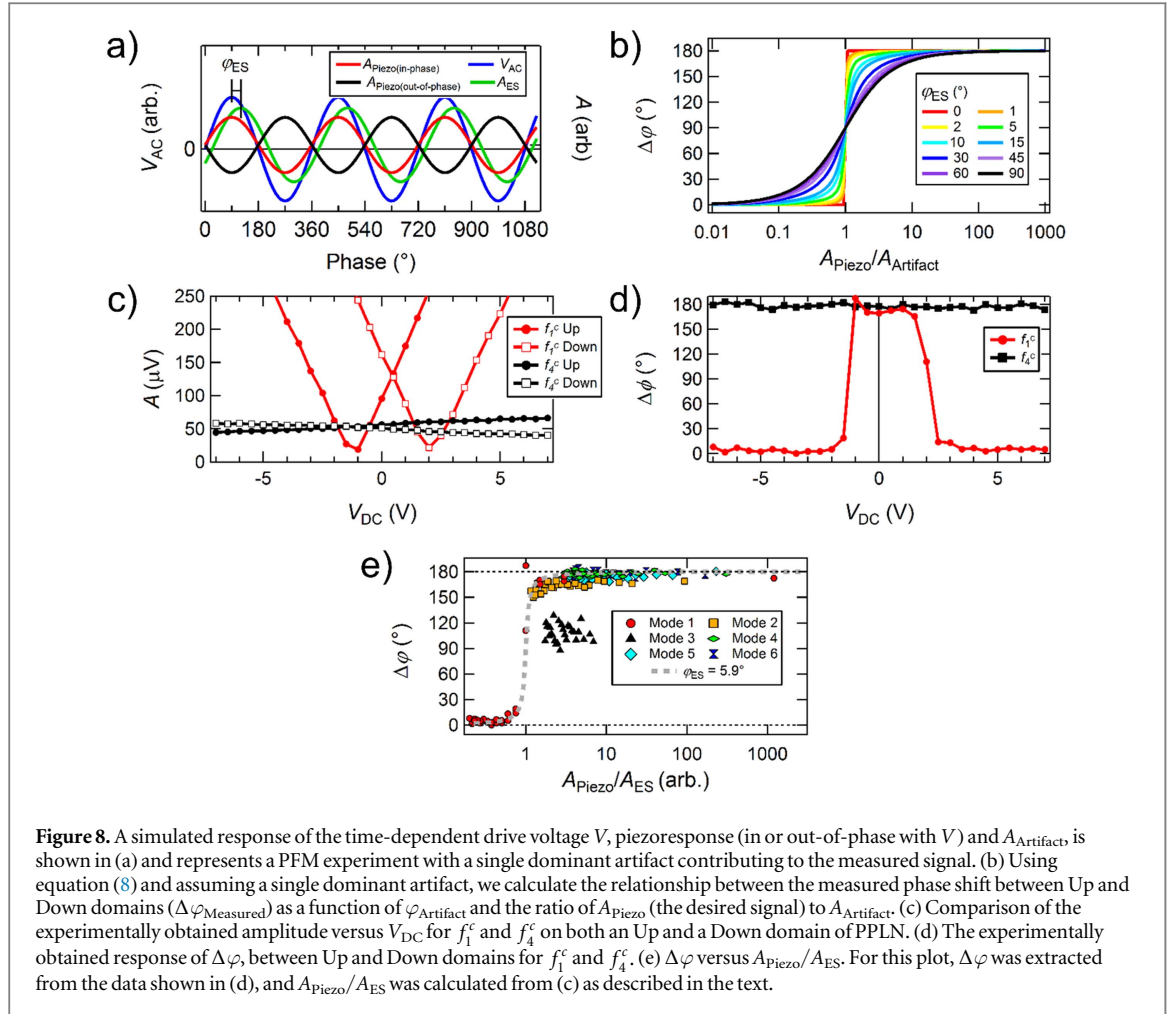
This approach cannot only improve status quo results, but can also enable accurate, artifact-free PFM on a greater range of materials and samples. Status quo PFM measurements require relatively stiff probes to minimize measurement artifacts. However, many material classes require the use of probes with lower k_{cant} values, which allows for increased force control and reduced sample damage and tip wear while simultaneously increasing lateral resolution. Here, we demonstrate that the use of higher frequency eigenmodes enables accurate PFM measurements with ‘soft’ probes that have k_{cant} values considerably lower than the current status quo PFM probe. In figures 6(e)–(h), we show the PFM results taken at f_1^c with a probe that has $\approx 5 \times$ lower k_{cant} than the ‘typical’ PFM probe. As expected, the f_1^c ($\approx 75 \text{ kHz}$) PFM results in figures 6(e) and (f) exhibit large measurement artifacts because of the low k_{cant} of the probe. The measured A values are $41\% \pm 7\%$ larger on the Down domains than the Up domains, and there is a readily observable increase in the A response from the top to the bottom of the image. This contrast in the slow-scan direction may be indicative of very long-range electrostatic artifacts, possibly as a result of localized charging of the surface by the electric fields present during the PFM measurement [23]. This is supported by the observation that the A signal is greatest when there is minimal overlap between the scanned area of the sample and the cantilever body. The probe orientation, relative to all images, is shown in the top right corner of figure 6(e). Furthermore, there is almost no phase contrast for these measurement conditions ($\Delta\varphi = \approx 1^\circ \pm 1^\circ$). The lack of phase contrast suggests that $A_{\text{piezo}} \ll A_{\text{total}}$.

DART-PFM data taken with the same probe, in the same sample location, but with $f_{\text{AC}} = f_4^c$ ($\approx 790 \text{ kHz}$), are shown in figures 6(g) and (h). Again, we observe a significant shift of the PFM response toward the ideal response. We observe similar amplitudes for the Up and Down domains, with $\Delta A = 9.35\% \pm 0.05\%$. Additionally, the phase shift is close to ideal ($183^\circ \pm 1^\circ$). This further highlights the value of using higher modes in order to collect accurate PFM data, and opens the door for accurate PFM measurements with an order of magnitude improved static force control.



To further study the artifact-minimizing capabilities of higher eigenmodes, we performed measurements on Up and Down PPLN domains with varying magnitudes of V_{AC} and V_{DC} . The variation of V_{AC} will affect the amplitude of all drive forces acting on the probe, whereas the variation of V_{DC} about a small range far below the writing voltage of PPLN will influence the electrostatic drive force (due to the DC term in the electrostatic force) without influencing the piezoresponse of the material. While performing the measurements in figure 6, some variation in frequency between domains was observed. Furthermore, tip-wear during the experiment and varying the V_{DC} can affect the frequency of the CR. Variations in frequency result in variations in the optical lever sensitivity of the cantilever (i.e., the cantilever shape factor [24]), and thus the apparent amplitude of the response. To ensure that changes in the cantilever shape factor do not influence our interpretation of apparent amplitude, all measurements were performed at a range of forces, which result in a range of CR frequencies for each eigenmode. We then interpolate the amplitude to a chosen frequency that is equal for all values of V_{DC} for the particular eigenmode order (see supplementary information: Shape Factor Compensation). Thus, the approach we present here is a robust approach to minimize shape-factor artifacts. Qualitatively, changing the selected value of f_n^c did not impact observed trends. The slopes of frequency-corrected A versus V_{AC} for f_1^c and f_4^c are shown in figures 7(a) and (b), respectively. The slope of a given line is representative (albeit in units of photodetector voltage rather than surface displacement distance) of the apparent piezo coefficient d_{app} of the material.

For f_1^c , figure 7(a), the slopes vary considerably over a DC bias range of ± 3 V, with a d_{app} maximum value of $250 \mu\text{V}/\text{V}$ at $V_{DC} = -3$ V and approximately nulled at $V_{DC} = 1.5$ V. We note that the DC voltage that corresponds to the maximum and minimum values of d_{app} are not equivalent on the Up versus Down domains. This highlights the parasitic influence electrostatic force can have on PFM measurements taken at f_1^c . For PFM measurements taken at f_4^c , figure 7(b), the slope range is from 34 to $30 \mu\text{V}/\text{V}$ across the same V_{DC} range, nearly independent of V_{DC} , thus showing several orders of magnitude reduction in uncertainty. In figure 7(c), we show the ratio of $\text{Max}(d_{app})/\text{Min}(d_{app})$, calculated from the shape corrected slope of A versus V_{AC} with V_{DC} varied between -3 and $+3$ V, for the first 5 eigenmodes. This ratio, which is indicative of the sensitivity of the measured



d_{app} value to electrostatic artifacts, rapidly approaches 1 with increasing eigenmode and strongly correlates with the reduction in amplitude error from BES forces predicted in figure 5(a).

Quantifying the increased piezoresponse in the apparent PFM signal with increased eigenmode order

Figures 6 and 7 indicate a substantial improvement in the reliability of the apparent PFM response by operating at higher-order eigenmodes. The data acquired with multiple modes show that enhanced sensitivity to desired piezo response or undesired BES artifacts can be achieved. Here, we show that based on the expected phase response of the PPLN sample, the fraction of apparent PFM signal attributed to surface strain can be quantitatively estimated. Figure 8(a) shows the relationship between the applied voltage V_{AC} and the response associated with $u(t)$ as well as the response of the artifact driven processes. For simplicity, figure 8(a) assumes that a single artifact process dominates the apparent response, though multiple signals contributing to the artifact response are possible. On any sample, φ_{Piezo} is expected to be in-phase or out-of-phase (i.e., shifted by 0° or 180° relative to the voltage signal) dependent upon whether the z -component of the local polarization is parallel or antiparallel to the polarization axis. The value of A_{Piezo} will depend only on the magnitude of the z -component of the polarization and not the sign. The artifact-driven cantilever response will result from a single, or multiple processes each with an associated A_{Artifact} and $\varphi_{\text{Artifact}}$ dependent upon the relative magnitudes of the drive forces listed above. The phase shift(s), $\varphi_{\text{Artifact}}$ will also depend upon numerous factors, is rarely known for a given system, and could vary significantly as a function of x - y position for a number of heterogeneous samples. In cases where there are only two main contributions to the measured PFM response, i.e. the piezoresponse of the sample and a single dominant artifact contribution (such as the situation shown in figure 8(a)), the φ measured by the lock-in-amplifier can be described by equation (10). We note that a similar equation can be derived for the case where multiple artifacts have comparable contributions to the measured signal.

$$\varphi_{\text{Measured}} = \tan^{-1} \left(\frac{A_{\text{Piezo}} \cos(\varphi_{\text{piezo}}) + A_{\text{ES}} \cos(\varphi_{\text{Artifact}})}{A_{\text{Piezo}} \sin(\varphi_{\text{piezo}}) + A_{\text{ES}} \sin(\varphi_{\text{Artifact}})} \right) \quad (10)$$

Thus, the difference in the phase response ($\Delta\varphi$) measured on Up versus Down domains on a sample such as PPLN, assuming a single dominant artifact contribution, can be calculated using

$$\Delta\varphi_{\text{Measured}} = \tan^{-1} \left(\frac{\beta \cos(\varphi_{\text{piezo}(2)}) + \cos(\varphi_{\text{Artifact}})}{\beta \sin(\varphi_{\text{piezo}(2)}) + \sin(\varphi_{\text{Artifact}})} \right) - \tan^{-1} \left(\frac{\beta \cos(\varphi_{\text{piezo}(1)}) + \cos(\varphi_{\text{Artifact}})}{\beta \sin(\varphi_{\text{piezo}(1)}) + \sin(\varphi_{\text{Artifact}})} \right), \quad (11)$$

where $\beta = \frac{A_{\text{Piezo}}}{A_{\text{Artifact}}}$.

Using equation (11), we calculate the relationship between the measured phase shift between Up and Down domains ($\Delta\varphi_{\text{Measured}}$) as a function of $\varphi_{\text{Artifact}}$ and the ratio of A_{Piezo} to A_{Artifact} . These relationships are shown in figure 8. As shown in figure 8(b), when $A_{\text{Piezo}}/A_{\text{Artifact}}$ is greater than ≈ 10 , $\Delta\varphi$ is only weakly dependent on $\varphi_{\text{Artifact}}$. Between $A_{\text{Piezo}}/A_{\text{Artifact}} = 10$ and $A_{\text{Piezo}}/A_{\text{Artifact}} = 0.1$ the sensitivity of the $\Delta\varphi$ versus $\varphi_{\text{Artifact}}$ increases rapidly when approaching $A_{\text{Piezo}}/A_{\text{Artifact}} = 1$ from either side. Finally, when $A_{\text{Piezo}}/A_{\text{Artifact}}$ is less than 0.1 the phase response becomes largely insensitive to both the presence of ferroelectric domains as well as variations in $\varphi_{\text{Artifact}}$. Thus, maintaining a ratio of $A_{\text{Piezo}}/A_{\text{ES}} > 10$ is desirable for collecting accurate A and φ data, and to avoid imaging contrast due to $\varphi_{\text{Artifact}}$, which is generally unknown and may vary as a function of x - y position on the sample.

Importantly, figure 8(b) demonstrates that **reliable φ data is a necessary but not sufficient condition for accurate A data**. That is to say, $\Delta\varphi$ less than 180° is indicative of error in the measured A signal, however $\Delta\varphi \approx 180^\circ$ can be observed in the presence of significant error in the A signal when $\Delta\varphi_{\text{Artifact}}$ is small. Values as low as $\Delta\varphi \approx 135^\circ$ have been reported for PFM measurements of PPLN samples using AFM probes with k_{cant} values in the 1–5 N m⁻¹ range (these k_{cant} values are typical for PFM measurements in the literature) [25]. We can use equation (8) to estimate $A_{\text{Piezo}}/A_{\text{Artifact}}$ for such a case. Interestingly, for $\Delta\varphi \approx 135^\circ$ the estimated values of $A_{\text{Piezo}}/A_{\text{Artifact}}$ are ≈ 1 to 2.5 depending on the value of $\varphi_{\text{Artifact}}$. Thus, only $\approx 50\%$ – 70% of the A signal is the result of the piezoresponse, with the remainder due to the electrostatic response.

To demonstrate the relationship between measured phase and electrostatic amplitude artifacts, we collected PFM point spectra on both Up and Down domains, with a constant V_{AC} , and varied the V_{DC} . Figure 8(c) shows the A versus V_{DC} response for f_1^c and f_4^c on both an Up and a Down domain. Because we assume that the piezoresponse is equivalent on the Up and Down domains, and the A response of f_1^c on Up and Down domains crosses at $V_{\text{DC}} \approx 0.5$ V, we conclude that the BES null voltage (V_{null}), which occurs when surface contact potential equals the DC bias is achieved when $V_{\text{DC}} \approx 0.5$ V. As shown, the sensitivity of A to V_{DC} , based on the slope of $\Delta A/\Delta V_{\text{DC}}$, is significantly larger for f_1^c as compared to f_4^c . This is another indication that the impact of electrostatic forces is greatly reduced at f_4^c relative to f_1^c , in agreement with figure 7. While f_1^c is strongly dominated by BES in this system, TES may contribute a significant fraction to the remaining slope of A versus V_{DC} in f_4^c . This is because the A due to F_{TES} is not expected to be reduced due to the increased dynamic stiffness of higher resonant modes (see figure 5(b)). We extracted the $\Delta\varphi$, between the Up and Down domains under these conditions, as shown in figure 8(d). While $\Delta\varphi \approx 180^\circ$ and is nearly constant between ± 7 V V_{DC} for f_4^c , the $\Delta\varphi$ at f_1^c is strongly dependent upon V_{DC} .

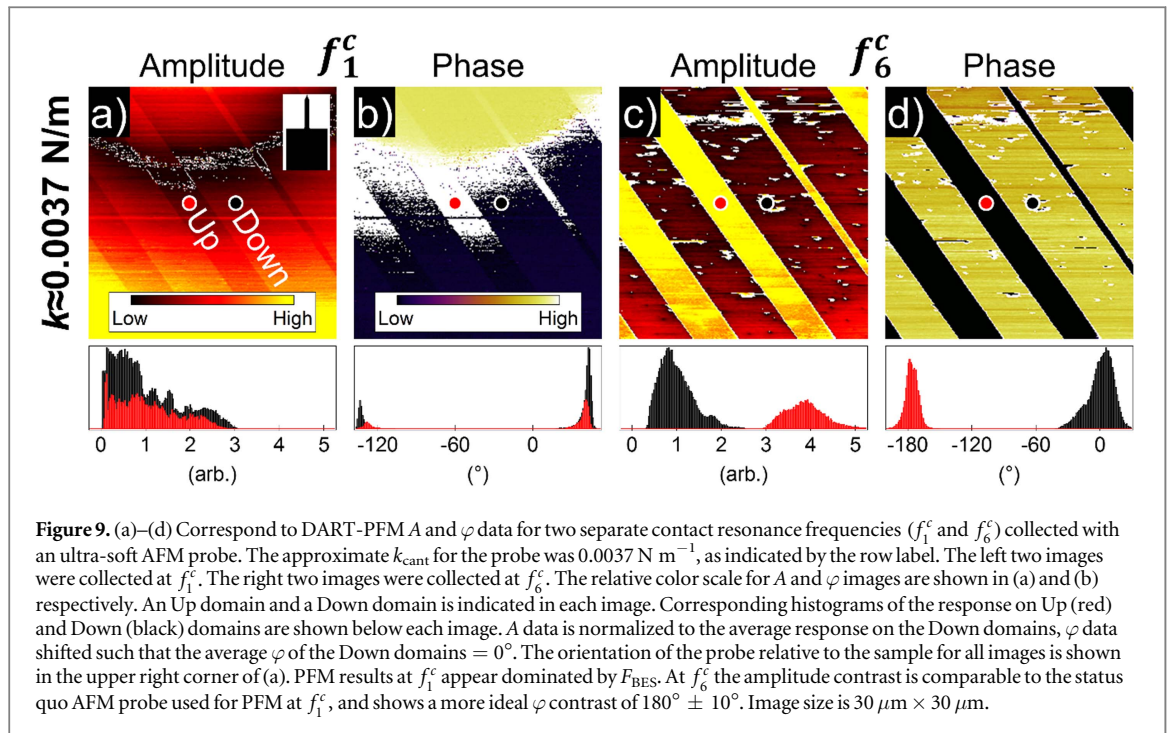
Using equation (11) and the A and $\Delta\varphi$ versus V_{DC} results, discussed for f_1^c and f_4^c above, the ratio of A_{Piezo} to A_{ES} was estimated for the first 6 eigenmodes across ± 7 V V_{DC} . For each mode, the intersection of A on the Up and Down domains was assumed to be the V_{DC} where A_{ES} is nulled, and thus $A = A_{\text{Piezo}}$. In order to estimate the value of A_{ES} at each V_{DC} the slope of the crossing sections of the A versus V_{DC} curves were each fit to a line. The value of A_{ES} was estimated by

$$A_{\text{ES}} = m(V_{\text{DC}} - V_{\text{null}}), \quad (12)$$

where m is the slope of A_{Measured} versus V_{DC} . Furthermore, the amplitude due to the piezoresponse of the sample can be estimated using

$$A_{\text{Piezo}} = A_{\text{Measured}} - A_{\text{ES}}. \quad (13)$$

Figure 8(e) is a plot of $\Delta\varphi$ versus $A_{\text{Piezo}}/A_{\text{ES}}$ estimated using equations (12) and (13), for the first 6 contact resonant modes. A few important trends can be observed from figure 8(e). First, with the exception of mode 3, the trend of the $\Delta\varphi$ versus $A_{\text{Piezo}}/A_{\text{ES}}$ results are approximately sigmoidal consistent with reduced A_{ES} with increasing mode. Furthermore, $\varphi_{\text{Artifact}} = 5.9^\circ$ can be estimated by fitting the multimodal $\Delta\varphi$ versus $A_{\text{Piezo}}/A_{\text{ES}}$. Thus, not only does this approach reduce the impact of electrostatic artifacts to the PFM measurement, it can also be used to extract $\varphi_{\text{Artifact}}$ which is difficult to estimate by other approaches, and is critical for estimating the remaining artifacts in the measurement. We note that the mode 3 results diverge considerably from the expected results. This was likely due to a low slope sensitivity at the position of the laser



spot for this mode under these conditions which lead to a relatively low amplitude signal relative to the background noise in the system.

Pushing the limits of low-force PFM with ultra-low stiffness cantilevers

After establishing that electrostatic artifact contributions to the measured amplitude A_{piezo} can be minimized by utilizing a higher eigenmode of a $k_{\text{cant}} \approx 0.3 \text{ N m}^{-1}$ cantilever, we sought to demonstrate that this approach is applicable to probes with even lower k_{cant} , enabling accurate measurements of piezoelectric coefficients even in very low stiffness materials such as polymers and biomaterials. To this end, we collected PFM data with an ultra-soft probe (BL-RC150VB, Olympus) which is typically used for extremely soft and fragile samples and in which tip-sample forces are limited to the picoNewton range, e.g. cells and DNA manipulation studies [26]. With a calibrated k_{cant} of only 0.0037 N m^{-1} this probe is *ca.* $440\times$ softer than the status-quo lever used in figure 6. With such a soft probe, the PFM signal at f_1^c ($\sim 65 \text{ kHz}$) is far from ideal, as shown in figures 9(a) and (b). The primary contrast in the A and φ data is between the top and the bottom of the image, indicating that the response is dominated by long-range electrostatic artifacts, as opposed to the piezoresponse of the sample. However, at f_6^c ($\approx 1.3 \text{ MHz}$), the top-to-bottom contrast in the A signal has been removed. There remains a large contrast between the amplitudes measured in the Up and Down domains that is not expected for an ideal piezoelectric response, with the A response on the Down domains being $70\% \pm 20\%$ smaller than the A response on the Up domains. We note that the Up domains show lower Q values and a broader f^c distribution (see supplementary information: DART-PFM Contact Resonance Frequency and Quality Factor Images). Further studies are needed to fully understand the nature of the nanomechanical response for ultra-soft probes, and how this response affects the measured value of A . However, the $\Delta\varphi$ ($180^\circ \pm 10^\circ$) matches the ideal piezoelectric phase shift for this system.

When we compare the results collected with the status quo probe (1.64 N m^{-1}) to the results collected with the ultra-soft probe (0.0037 N m^{-1}), the great potential benefit of using higher-frequency modes for PFM studies becomes obvious. As we have discussed, it is current practice in the PFM field (as illustrated by many recent publications) to use a probe with similar, or greater, k_{cant} than our status quo probe, and to take the measurements with a drive frequency at or below f_1^c . We have demonstrated comparable A contrast ($70\% \pm 20\%$ versus $77\% \pm 7\%$), and improved phase contrast ($180^\circ \pm 10^\circ$ versus $162^\circ \pm 5^\circ$) for the ultra-soft probe at f_6^c relative to the status-quo probe at f_1^c . We note that using the ultra-soft probe results in wider distributions of the measured amplitudes and phases, as evident in the histogram data. This may be due to the greatly reduced static tip-sample contact force, which is likely to result in temporary loss of contact while the tip is scanned over small, loosely held particulate features on the surface, e.g. dust or contamination that would be laterally displaced by the probe tip for a higher k_{cant} cantilever. Clearly, the increased width of the amplitude and phase distribution is not ideal. However, for soft samples, this disadvantage is far outweighed by the approximately two-to-three orders of magnitude increase in force control. This will result in the extension of

PFM and related methods to a wide class of materials that are too fragile to allow accurate PFM measurements with status-quo PFM probes.

Conclusions

Through modeling and experimental studies, we have demonstrated that the use of higher frequency resonance modes in PFM measurements brings a number of benefits. Modeling up to the first 6 eigenmodes, these benefits include an increase in the maximum measurement sensitivity (>1 order of magnitude increase in amplitude sensitivity), reduced electrostatic artifacts in the response (>60 fold reduction in F_{BES} artifacts for a 0.3 N m^{-1} probe), and greater than an order of magnitude difference in sensitivity to lateral coupling to the flexural mode between modes 3 and 6. Furthermore, we have demonstrated that the use of higher eigenmodes of status-quo probes ($k_{\text{cant}} = 1\text{--}5 \text{ N m}^{-1}$) greatly reduces the magnitude of electrostatic artifacts, without any specialized hardware. This approach additionally was shown to enable improved measurement accuracy with probes that are 10 or even 1000 times softer than the status-quo probes. For example, through analysis of the phase response of measurements using soft probes ($k_{\text{cant}} \approx 0.3 \text{ N m}^{-1}$) we can estimate that measurement artifacts make up greater than 90% of the measured amplitude signal at f_1^c and the normal piezoresponse makes up less than 10% of the amplitude signal. This proportion can be inverted, resulting in reliable PFM measurements, simply by measuring the PFM response at f_4^c . We have gone on to show how we can combine the high mode approach with shape factor normalization, allowing direct comparison of the uncertainty in surface strain amplitude. These approaches not only improve the reliability of the amplitude contrast in PFM measurements, but also increase the reliability of the measured phase response. For researchers seeking to utilize higher cantilever eigenmodes to improve data reliability in PFM and related techniques, we recommend some simple guidelines. When observing interesting or unexpected behavior (e.g. in amplitude or phase) between domains, repeating the measurement at a higher eigenmode can provide increased confidence in whatever conclusions are drawn. Researchers should seek convergence of the observed phenomena as artifacts are reduced with increased eigenmode order. Finally, if higher modes are not immediately detected, a simple translation of the detection laser along the cantilever body may reveal a previously hidden eigenmode. Failure to observe the higher eigenmodes, even with modifications to detection laser position, should be seen as a warning that observed contrasts may be charge based, rather than electromechanical, or the electromechanical response may be strongly frequency dependent. Overall, we have demonstrated approaches that greatly improve the reliability and accuracy of PFM measurements, enable the use of soft and ultra-soft probes for quantitative PFM studies of a wider class of materials, and do not require specialized hardware or customized AFM probes.

Acknowledgments

Publication of NIST, an agency of the US government, not subject to copyright in the United States. This research was performed while GAM held a National Research Council Research Associateship Award at the National Institute of Standards and Technology. Commercial equipment, instruments, or materials are identified only in order to adequately specify certain procedures. In no case does such identification imply recommendation or endorsement by the National Institute of Standards and Technology, nor does it imply that the products identified are necessarily the best available for the purpose.

ORCID iDs

Jason P Killgore  <https://orcid.org/0000-0002-8458-6680>

References

- [1] Vasudevan R K, Balke N, Maksymovych P, Jesse S and Kalinin S V 2017 Ferroelectric or non-ferroelectric: why so many materials exhibit 'ferroelectricity' on the nanoscale *Appl. Phys. Rev.* **4** 21302
- [2] Setter N *et al* 2006 Ferroelectric thin films: review of materials, properties, and applications *J. Appl. Phys.* **100** 51606
- [3] Hermes I M *et al* 2016 Ferroelastic fingerprints in methylammonium lead iodide perovskite *J. Phys. Chem. C* **120** 5724–31
- [4] Anon 2016 The Nobel Prize in Chemistry 2016 [Nobelprize.org](https://www.nobelprize.org)
- [5] Balke N, Jesse S, Kim Y, Adamczyk L, Ivanov I N, Dudney N J and Kalinin S V 2010 Diffusion processes in ionically-scale *ACS Nano* **4** 7349–57
- [6] Morozovska A N, Eliseev E A and Kalinin S V 2010 Electromechanical probing of ionic currents in energy storage materials *Appl. Phys. Lett.* **96** 222906
- [7] Balke N, Maksymovych P, Jesse S, Kravchenko I I, Li Q and Kalinin S V 2014 Exploring local electrostatic effects with scanning probe microscopy: implications for piezoresponse force microscopy and triboelectricity *ACS Nano* **8** 10229–36

- [8] Miao H, Tan C, Zhou X, Wei X and Li F 2014 More ferroelectrics discovered by switching spectroscopy piezoresponse force microscopy? *Europhys. Lett.* **108** 27010
- [9] Gomez A, Puig T and Obradors X 2018 Diminish electrostatic in piezoresponse force microscopy through longer or ultra-stiff tips *Appl. Surf. Sci.* **439** 577–82
- [10] Killgore J P and Hurley D C 2012 Low-force AFM nanomechanics with higher-eigenmode contact resonance spectroscopy *Nanotechnology* **23** 55702
- [11] Melcher J, Hu S and Raman A 2007 Equivalent point-mass models of continuous atomic force microscope probes *Appl. Phys. Lett.* **91** 1–4
- [12] Bradler S, Schirmeisen A and Roling B 2017 Amplitude quantification in contact-resonance-based voltage-modulated force spectroscopy *J. Appl. Phys.* **122** 65106
- [13] Seal K, Jesse S, Rodriguez B J, Baddorf A P and Kalinin S V 2007 High frequency piezoresponse force microscopy in the 1–10 MHz regime *Appl. Phys. Lett.* **91** 232904
- [14] Bradler S, Kachel S R, Schirmeisen A and Roling B 2016 A theoretical model for the cantilever motion in contact-resonance atomic force microscopy and its application to phase calibration in piezoresponse force and electrochemical strain microscopy *J. Appl. Phys.* **120** 165107
- [15] Molotskii M, Agronin A, Urenski P, Shvebelman M, Rosenman G and Rosenwaks Y 2003 Ferroelectric domain breakdown *Phys. Rev. Lett.* **90** 4
- [16] Zhou Q, Lau S, Wu D and Kirk Shung K 2011 Piezoelectric films for high frequency ultrasonic transducers in biomedical applications *Prog. Mater. Sci.* **56** 139–74
- [17] Wagner R and Killgore J 2017 Reconstructing the distributed force on an atomic force microscope cantilever *Nanotechnology* **28** 104002
- [18] Balke N, Eliseev E A, Jesse S, Kalnaus S, Daniel C, Dudney N J, Morozovska A N and Kalinin S V 2012 Three-dimensional vector electrochemical strain microscopy *J. Appl. Phys.* **112** 052020
- [19] Rodriguez B J, Callahan C, Kalinin S V and Proksch R 2007 Dual-frequency resonance-tracking atomic force microscopy *Nanotechnology* **18** 475504
- [20] Gannepalli A, Yablon D G, Tsou A H and Proksch R 2013 Corrigendum: mapping nanoscale elasticity and dissipation using dual frequency contact resonance AFM *Nanotechnology* **24** 159501
- [21] Proksch R 2015 *In-situ* piezoresponse force microscopy cantilever mode shape profiling *J. Appl. Phys.* **118** 072011
- [22] Jungk T, Hoffmann A and Soergel E 2006 Quantitative analysis of ferroelectric domain imaging with piezoresponse force microscopy *Appl. Phys. Lett.* **89** 163507
- [23] Balke N, Jesse S, Carmichael B, Okatan M B, Kravchenko I I, Kalinin S V and Tselev A 2017 Quantification of in-contact probe-sample electrostatic forces with dynamic atomic force microscopy *Nanotechnology* **28** 65704
- [24] Balke N, Jesse S, Yu P, Carmichael B, Kalinin S V and Tselev A 2016 Quantification of surface displacements and electromechanical phenomena via dynamic atomic force microscopy *Nanotechnology* **27** 425707
- [25] Proksch R 2015 *In-situ* piezoresponse force microscopy cantilever mode shape profiling *J. Appl. Phys.* **118** 72011
- [26] Churnside A B, Sullan R M A, Nguyen D M, Case S O, Bull M S, King G M and Perkins T T 2012 Routine and timely sub-piconewton force stability and precision for biological applications of atomic force microscopy *Nano Lett.* **12** 3557–61